BILINGUAL PUBLISHING CO.
Pioneer of Global Academics Since 1984

Journal of Geological Research
https://ojs.bilpublishing.com/index.php/jgr-a

ARTICLE

Characterization of the Sulfide Deposits in the Southeastern Nigeria Using VLF Method: Insights from Numerical Modeling and Field Examples

D. E. Falebita[1] O. Afolabi[1] B. O Soyinka[2] A. A. Adepelumi[1*]

1.Department of Geology, Obafemi Awolowo University, Ile-Ife, Nigeria
2.Terracon, Seattle, Washington DC, USA.

ARTICLE INFO

Article history
Received: 15 January 2021
Accepted: 24 February 2021
Published Online: 31 March 2021

Keywords:
Sulfide
Conductor
VLF
Overburden thickness
Polarization parameters
Nigeria

ABSTRACT

A priori geologic and geophysical information has been used to construct conceptual VLF experiments on conductively and inductively coupled overburden geological models of the lead-zinc (Pb-Zn) mineralization zone found in southeastern Nigeria. This is based on the finite element approach to (1) simulate different geologic situations of overburden occurrence, (2) examine the roles played by overburden in modifying and masking VLF responses of a buried conductor target, and (3) confirm the effectiveness of VLF method in mapping lead-zinc lodes found in sedimentary terrains. The computed theoretical model curves and field examples are expected to serve as guide for VLF anomaly pattern recognition due to overburden thickness, resistivity and width of conductor in similar terrain as the study area.

1. Introduction

Mining of the sulfide minerals in Abakaliki area of southeastern Nigeria started in the early nineteenth century culminating a total of 9000 tons of lead ore and 1000 tons of zinc ore mined during the peak periods between 1946 and 1974. Various geophysical and geochemical methods have been used in prospecting for economic sulfide lodes in the area. However, very low frequency (VLF) geophysical method was only recently used [1, 2]. The VLF method is a classic electromagnetic method that has been used worldwide for decades as a geophysical prospecting tool [3, 4, 5, 6, 7, 8, 9, 10, 11, 12, 13]. Electrically conductive mineralized zones are generally more conductive than the host rocks in which they are emplaced, so ore targets can be delineated with ease using the VLF method [3, 5, 14]. The method is attractive to mineral explorationists because of its cost-effectiveness, speed of operation and portability of the equipment [15, 16, 1, 17, 18].

One of the up-hill tasks usually encountered while interpreting acquired VLF data is differentiating between anomalies caused by the ore bodies and conductively coupled overburden EM anomalies that are usually regarded as geological noise. On the other hand, EM signatures of promising anomalous zones are often masked by inductively coupled overburden leading to quantify such zones

**Corresponding Author:*
A. A. Adepelumi,
Department of Geology, Obafemi Awolowo University, Ile-Ife, Nigeria;
Email: adepelumi@gmail.com

 DOI: https://doi.org/10.30564/jgr.v3i1.2809

as non-promising and/or non-economic. For example, [1] reported lack of continuity of VLF response along some of their profiles despite the fact that the area is known to be highly mineralized. So, we deem it necessary to conduct numerical VLF model studies in order to investigate the roles played by overburden in masking and/or modifying the VLF response of a buried mineralized target and the effect of ore size to VLF signatures. Although several authors in the past have studied the effect of a uniform overburden on EM responses of a basement conductor [19, 20, 21, 22], no one has investigated VLF responses of conductors found in sedimentary terrain having similar geology to our research site in Nigeria. We hope that the geometry of the synthetic models will simulate the exploration target and serve as a guide in identifying such anomalous bodies in field situations specific to the study area in the southeastern Nigeria.

2. Geological Settings

The Abakaliki sulfide mineralization is found within the Cretaceous shales of the Asu River Group in the lower part of the Benue trough of Nigeria [23]. The Asu River Group represents the earliest sediments (shale and sandy-shale) that were deposited unconformably on the subsiding basement topographical depressions during the first marine transgressions into the trough [23, 24]. The emplacement of the mineralization is thought to be tectonically controlled [25]. The primary minerals constituting the lode are galena and sphalerite while the secondary minerals include pyrite, siderite, marcasite, limonite and quartz [1]. Formation temperature of the mineralization has been estimated to be about 140 ^{o}C while its origin is hydrothermal. Source of the lead mineralization is the detrital alkali feldspars which were eroded from the Precambrian basement and re-concentrated [26]. The age of the mineralization is generally agreed to take place at the end of the Santonian [27, 28, 29, 23]. According to [23], the formation of the mineralization took place in three distinct stages: (1) pre-ore fracturing and brecciation of Albian shales accompanied by the precipitation of framboidal and colloform aggregates of pyrite, siderite and quartz; (2) ore stage formation of sphalerite, galena, copper bearing minerals; and (3) final deposition of octahedral galena, sphalerite, bravoite and marcasite in the hanging wall of the veins.

3. The VLF-EM Overview

The VLF-EM principle is based on receiving and interpreting transmitted long distance electromagnetic signals from mainly military and navigation radio transmitters around the world. The frequency ranges can be very low, 3-30 kHz and low, 30-300 kHz [30]. The remote transmitter radiates two-component primary EM field - a vertical electric field component and a horizontal magnetic field component each perpendicular to the direction of propagation. These fields induce electric currents in conductive bodies lying below earth's surface to produce secondary magnetic fields that can be detected at the surface through deviation of the normal radiated field by the VLF receiver [31]. One part of the secondary field oscillates in-phase (real component) and the other part oscillates out-of-phase (imaginary) with respect to the primary field [32, 33, 13]. The oscillation traces an elliptic polarization of the primary field whose penetration depth depends on the transmitter frequency and the electric resistivity of the ground governed by skin depth relation:

$$\delta = 503\left(\frac{\rho}{f}\right)^{1/2}, \tag{1}$$

where ρ is the electrical resistivity in Ωm, f is the frequency in Hz and δ is the skin depth in meters [34, 9].

4. Numerical Modelling of VLF Data

We evaluate, through numerical modeling experiments, the VLF responses due to moderate overburden layer of uniform thickness, moderate conductivity, and finite lateral extent which is in galvanic contact (Model 1), and non-galvanic contact (Model 2), with a vertical planar conductor (ore-body) lying below it. This is because electromagnetic conductors of interest may be overlain by a partially conducting overburden layer which maybe or not in galvanic contact [21] with the underlying mineralized lead-zinc ore-body. The modeling is carried out with the sole aim of obtaining better insight into characteristics of the VLF responses that will help in explaining the possible role played by overburden in masking VLF responses when the overburden is conductively, and inductively coupled to the underlying ore body target. The working assumption is that the VLF signal of frequency 16 kHz from the transmission station at Great Britain is detectable in the study area [1]. The first set of VLF responses of interest is (1) the tilt angle (θ), which is the inclination of the major axis of the polarization ellipse, and (2) ellipticity (e) known as the ratio of the minor to the major axis of the ellipse [35] using relations proposed by [36].

$$\tan 2\theta = \pm \frac{2\left(H_z/H_x\right)\cos\Delta\phi,}{1-\left(H_z/H_x\right)^2} \tag{2}$$

DOI: https://doi.org/10.30564/jgr.v3i1.2809

$$e = \frac{H_z H_x \sin \Delta\phi}{H_1^2}, \quad (3)$$

where H_z and H_x are the amplitudes, the phase difference $\Delta\varphi = \varphi_z - \varphi_x$, in which φ_z is the phase of H_z and φ_x is the phase of H_x and $H_1 = \left| H_z e^{i\Delta\varphi} \sin\theta + H_x \cos\theta \right|$ [37]. Interpretation is based on [38] that showed that the inflection point of the tilt-angle and ellipticity signature will centre right on top of the conductor and the separation of the peak-peak amplitude of the response is an indirect indicator of the depth of burial of the conductor. The second set of VLF responses is the apparent resistivity (ρ_a) and the corresponding phase angle (φ) [39] using the relations proposed by [40, 41].

$$\rho_a = \frac{1}{\omega\mu}\left|\frac{E_y}{H_x}\right|^2, \quad (4)$$

$$\varphi = \arctan\left[\frac{\mathrm{Im}\left(E_y / H_x\right)}{\mathrm{Re}\left(E_y / H_x\right)}\right], \quad (5)$$

where ω the angular frequency of the VLF primary is field and μ is the magnetic permeability of the subsurface [37]. Low resistivity zones are interpreted as possible fracture zones. The third set is the computation of equivalent current density (equation 6) for the conductive and inductive overburden models by linear filtering [42] of the real component of the secondary field. The filtering was by using the program developed by KIGAM [43, 44] to show the distribution of current with depth and the effect of overburden variation on the detectability of the conductor. This process leads to enhancement of anomalous signature, provides indication of current concentrations and spatial distribution that approximately reflect the depth and location of subsurface conductor [42, 43, 45].

$$I_a(0) = \frac{2\pi\left(-0.102 \cdot H_{-3} + 0.059 \cdot H_{-2} - 0.561 \cdot H_{-1} + 0.561 \cdot H_1 - 0.059 \cdot H_2 + 0.102 \cdot H_3\right)}{z} \quad (6)$$

where I_a is the equivalent current at a specific position and depth z; H_{-3} through H_3 are the originally computed synthetic VLF data.

The models used in the study closely approximate the electric structure beneath the survey lines used by [1] where the ore-body is either 10 m or 20 m wide [27, 23] and has 30 m length (Figure 2). A resistivity value of 0.01 Ωm was assigned to the lead-zinc lode based on the conductivity of the lode obtained by [27, 23]. The ore is considered to have a dip angle of 90° [1, 29] and embedded in a half-space of resistivity 40 Ωm overlain by an overburden of changing resistivity values between 50 and 500 Ωm [26] . A 200 m long survey line was considered and all responses of the mineralized zone are computed at a fixed frequency of 16 kHz every 2 m using a 100-mesh in x-direction and 30-mesh in y-direction making a total of 3000 elements.

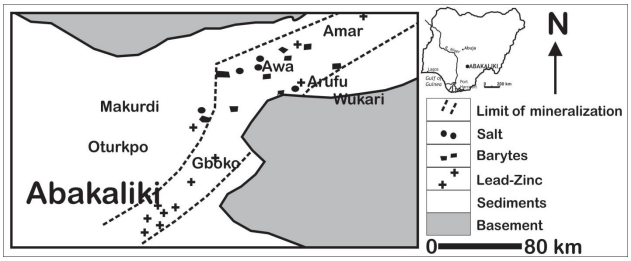

Figure 1. An illustrative description of the Lead-Zinc mineralization of the southeastern Nigeria (modified after Cratchley and Jones, 1965).

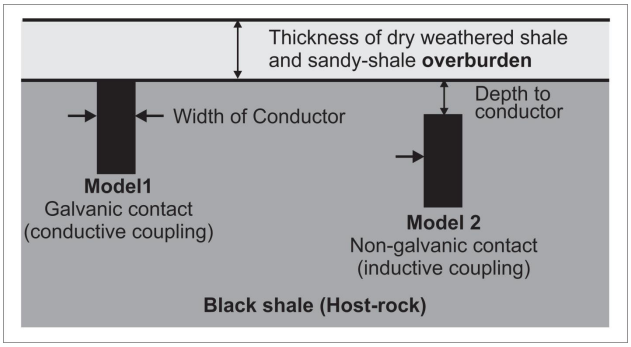

Figure 2. Description of the model configuration. A finitely conducting ore-body overlain by (1) conductively coupled and (2), inductively coupled uniform overburden layer.

4.1 Model 1 – Conductively Coupled

The ore-body with resistivity of 0.01 Ωm was allowed to have galvanic contact (*conductively coupled*) with the overburden of 10 m, 20 m and 30 m thickness and a host rock resistivity of 40 Ωm while the polarization parameters (apparent resistivity, phase, tilt and ellipticity) were computed for changes in overburden resistivity at 50, 100, 200 and 500 Ωm respectively.

4.2 Model 2 – Inductively Coupled

The ore-body was fixed at a depth of 4 m *inductively coupled* with overburden layer of 50 Ωm resistivity and changing thickness of 10 m, 20 m and 30 m. The resistivity values of the host rock and the ore body are the same as in model 1. These resistivity values correspond to those

 DOI: https://doi.org/10.30564/jgr.v3i1.2809

of the weathered shale and sandy-shale found in Abakaliki area. While keeping these parameters constant, the polarization parameters were computed for ore-body width of 10 m and 20 m respectively.

5. Results and Discussion

5.1 The VLF Synthetic Polarization Responses

Figure 3 and 4 show the various curves of the VLF synthetic polarization responses for models 1 and 2. For model 1 (Figs. 3a, b, c and d), the conductor is conductively coupled with overburden (galvanic contact), where the resistivity of the overburden varies as 50 Ωm, 100 Ωm, 200 Ωm and 500 Ωm respectively. For model 2 (Figs. 4a and 4b), the conductor is inductively coupled with the overburden (non-galvanic contact). All the polarization parameters, that is, apparent resistivity (expressed in Ωm), phase (expressed in degrees), tilt angle and ellipticity (expressed in percentages) have distinct and diagnostic characteristics of the buried conductor at different resistivity values and thicknesses of the overburden. Tables 1 and 2 summarize the polarization parameters for models 1 and 2 respectively.

5.1.1 Model 1 - Overburden Resistivity of 50 Ωm

Figure 3a shows the curves of the polarization parameters for overburden resistivity of 50 Ωm. At 10 m of overburden, the resistivity values across the buried conductor vary between 17.68 and 48.79 Ωm with an amplitude difference of about 31.12 Ωm. The lowest value is centered on the conductor and the highest values are representative of the host rock. The phase values vary between 46.94 and 77.96 degrees with amplitude of about 31.03 degrees. The peak of the curve is centered on the conductor. The tilt values vary between -8.49% and 8.54% with a difference of about 17.03%. The crossover point from the positive peak to negative peak is centered on the conductor. The ellipticity values vary between -0.18% and 0.18% with a difference of 0.36%. Similar to the tilt, the crossover point from the positive peak to negative peak is centered on the conductor. At 20 m of overburden, resistivity values vary between 49.16 and 54.33 Ωm with a reduced interval (about 5.16 Ωm) compared to 10 m overburden thickness. Similarly, the phase values vary between 46.31 and 61.48 degrees with a reduced interval of 15.17 degrees. The tilt varies between -1.59% and 1.59% with an interval of 3.17% while the ellipticity varies between -0.08% and 0.08% with an interval of 0.15%. At 30 m of overburden, the resistivity varies between 50.72 Ωm and 57.99 Ωm with an interval 7.27 Ωm. The resistivity distribution at this depth is different from those at 10 and 20 m overburden in that the peak of the curve is centered on the conductor indicating that the resistivity of the conductor is completely masked at greater depth. The phase varies between 45.31 and 50.22 degrees with a reduced interval of 4.92 degrees. The tilt varies between -1.31% and 1.32% with an interval of 2.63% and the ellipticity varies between -0.02% and 0.02% at an interval of 0.04%. The crossover points between the positive peaks and negative peaks are centered on the conductor. The tilt curve at this depth shows reverse shape compared to shallower depths. The reduction in the range (interval) of values of the polarization parameters at 20 m and 30 m is an indication of VLF attenuation/masking/screening at greater depths.

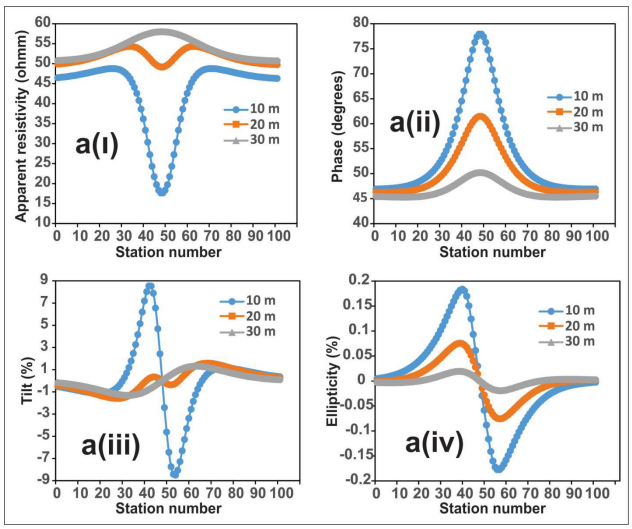

Figure 3a. Computed polarization parameters for a buried conductor model 1 for overburden resistivity of 50 ohm-m, and overburden thicknesses of 10, 20 and 30 m. The upper left panel show resistivity a(i), upper right panel show phase a(ii), lower left panel show the tilt angle a(iii) while the lower right panel show the ellipticity a(iv).

5.1.2 Model 1 - Overburden Resistivity of 100 Ωm

Figure 3b shows the polarization parameters for overburden resistivity of 100 Ωm. The resistivity across the buried conductor varies between 18.64 and 64.58 Ωm with amplitude of about 45.94 Ωm at 10 m. It varies between 65.41 and 88.18 Ωm with a difference of 22.79 Ωm at 20 m; and varies between 99.50 and 105.95 Ωm with a difference of 6.44 Ωm at 30 m. Clearly amplitude of the resistivity is decreasing with increasing depth. The phase varies between 52.60 and 81.60 degrees with a difference of 29.01 degrees at 10 m. It varies between 52.93 and 70.77 degrees with a difference of 17.83 degrees at 20 m and varies between 50.60 and 59.94 degrees with a difference of 9.34 degrees at 30 m. The peaks of the curves are

DOI: https://doi.org/10.30564/jgr.v3i1.2809

centered on the conductor. The tilt varies between -10.68 and 10.95% with a difference of 21.63% at 10 m. It varies between -2.38 and 2.35 with amplitude difference of 4.73% at 20 m and varies between -1.16 and 1.16% with amplitude difference of 2.33% at 30 m. The crossover points from the positive peak to negative peak are centered on the conductor. Apart from reduction in amplitude at greater depths, the tilt curve at 30 m is reversed possibly due to masking by the overburden. The ellipticity varies between -0.17 and 0.18% with amplitude difference of 0.36 at 10 m. It varies between -0.10 and 0.10 with a difference of 0.20 at 20 m and varies between -0.05 and 0.05 with difference of 0.09 at 30 m. Similar to the tilt, the crossover points between the positive and negative peaks are centered on the conductor.

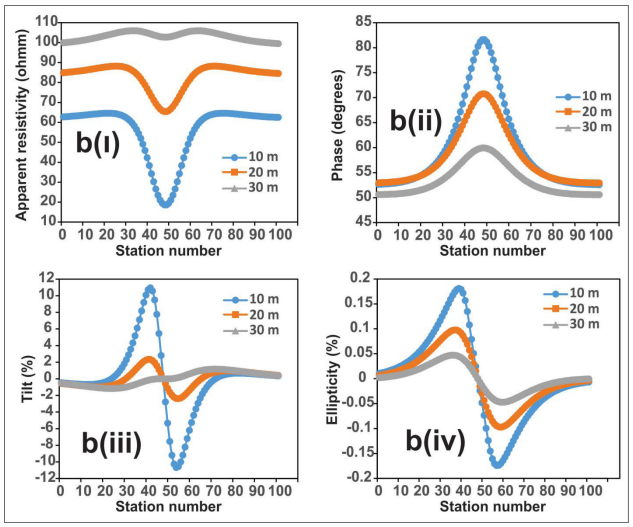

Figure 3b. Computed polarization parameters for a buried conductor model 1 for overburden resistivity of 100 ohm-m, and overburden thicknesses of 10, 20 and 30 m. The upper left panel show resistivity b(i), upper right panel show phase b(ii), lower left panel show the tilt angle b(iii) while the lower right panel show the ellipticity b(iv).

5.1.3 Model 1 - Overburden Resistivity of 200 Ωm

Figure 3c shows the polarization parameters for overburden resistivity of 200 Ωm. The resistivity across the buried conductor varies between 19.07 and 74.70 Ωm with a difference of about 55.63 Ωm at 10 m. It varies between 74.03 and 117.18 Ωm with a difference of 43.15 Ωm at 20 m; and varies between 139.84 and 160.93Ωm with a difference of 21.09 Ωm at 30 m. Again, the amplitude of the resistivity is decreasing with increasing depth. The phase varies between 56.39 and 83.56 degrees with a difference of 27.17 degrees at 10 m. It varies between 59.34 and 77.07 degrees with a difference of 17.74 degrees at 20 m and varies between 58.30 and 69.62 degrees with a difference of 11.32 degrees at 30 m. The peaks of the curves are centered on the conductor. The tilt varies between -11.79 and 12.12% with a difference of 23.90% at 10 m. It varies between -4.10 and 4.09% with amplitude difference of 8.189% at 20 m and varies between -1.09 and 1.07% with amplitude difference of 2.15% at 30 m. The crossover points from the positive peak to negative peak are centered on the conductor. There is no reversal of the tilt curve at 30 m compared to previous one. The ellipticity varies between -0.17 and 0.17% with amplitude difference of 0.34% at 10 m. It varies between -0.10 and 0.10% with a difference of 0.20% at 20 m and varies between -0.06 and 0.06% with a difference of 0.13 at 30 m. The crossover points between the positive and negative peaks are centered on the conductor.

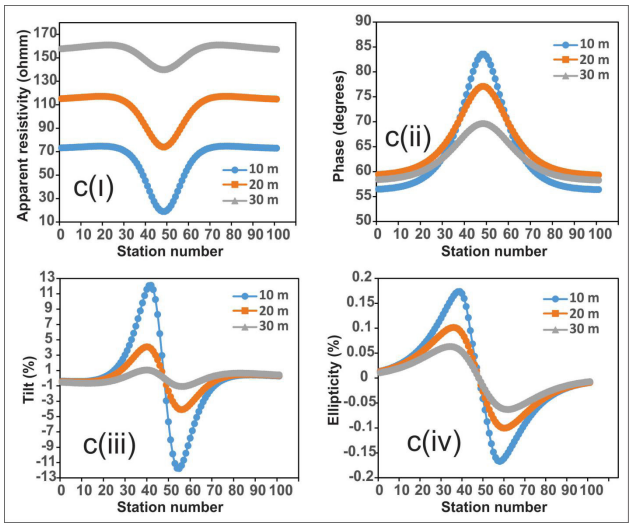

Figure 3c. Computed polarization parameters for a buried conductor model 1 for overburden resistivity of 200 ohm-m, and overburden thicknesses of 10, 20 and 30 m. The upper left panel show resistivity c(i), upper right panel show phase c(ii), lower left panel show the tilt angle c(iii) while the lower right panel show the ellipticity c(iv).

5.1.4 Model 1 - Overburden Resistivity of 500 Ωm

Figure 3d shows the polarization parameters for overburden resistivity of 500 Ωm. The resistivity across the buried conductor varies between 19.29 and 81.50 Ωm with a difference of about 62.21 Ωm at 10 m. It varies between 78.54 and 139.41 Ωm with a difference of 60.87 Ωm at 20 m; and varies between 163.31 and 211.47 Ωm with a difference of 48.16 Ωm at 30 m. The amplitude of the resistivity is decreasing with increasing depth. The phase varies between 59.04 and 84.78

DOI: https://doi.org/10.30564/jgr.v3i1.2809

degrees with a difference of 25.74 degrees at 10 m. It varies between 64.74 and 81.43 degrees with a difference of 16.69 degrees at 20 m and varies between 66.45 and 77.77 degrees with a difference of 11.32 degrees at 30 m. The peaks of the curves are centered on the conductor. The tilt varies between -12.45 and 12.83% with a difference of 25.28% at 10 m. It varies between -5.28 and 5.31% with amplitude difference of 10.59% at 20 m and varies between -2.38 and 2.38% with amplitude difference of 4.76% at 30 m. The crossover points from the positive peak to negative peak are centered on the conductor. There is no reversal of the tilt curve at 30 m compared to previous one. The ellipticity varies between -0.16 and 0.17% with amplitude difference of 0.33% at 10 m. It varies between -0.10 and 0.10% with a difference of 0.19% at 20 m and varies between -0.07 and 0.07% with a difference of 0.13 at 30 m. The crossover points between the positive and negative peaks are centered on the conductor.

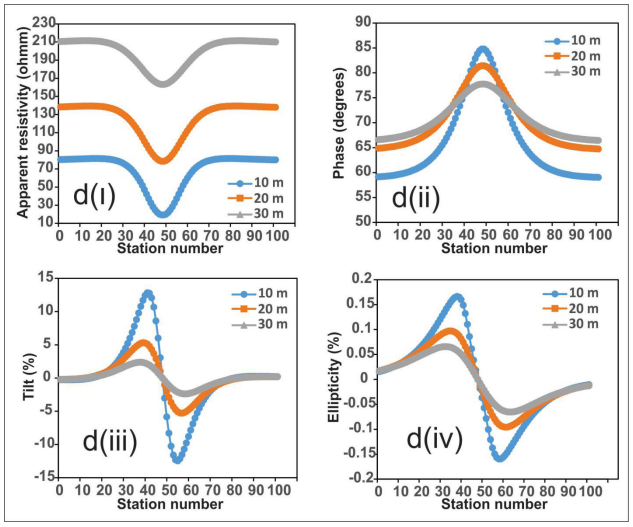

Figure 3d. Computed polarization parameters for a buried conductor model 1 for overburden resistivity of 500 ohm-m, and overburden thicknesses of 10, 20 and 30 m. The upper left panel show resistivity d(i), upper right panel show phase d(ii), lower left panel show the tilt angle d(iii) while the lower right panel show the ellipticity d(iv).

5.2 Model 2 - Overburden Resistivity of 50 Ωm

Figures 4a and 4b show the polarization curves for the inductively coupled model of overburden resistivity 50 Ωm with a conductor buried at 4 m below the overburden. Figure 4a is specifically for conductor width of 10 m while Figure 4b is for conductor width of 20 m. Similar anomaly patterns and shapes are observed over the buried ore-body as in conductive model at the same overburden resistivity of 50 Ωm (Fig. 3a) except for some differences. First, the amplitude of the resistivity is higher in the inductive model than the conductive model at the same overburden thickness. This is expected because for the conductive model, there is contact with the overburden but there is no contact with the overburden in the inductive model. The space of no contact is a low conductivity space for the inductive model which in turn increases resistivity. Second, the behaviour of the phase is the reverse of that of the resistivity in that the amplitude of the phase is higher in conductive model (Fig. 3b(i)) than the inductive model (Fig. 4b(i)) for the same overburden thickness. Third, the tilt amplitude in the inductive model is higher than that of the conductive model while the ellipticity values of the two models are about the same. When the width of the conductor is increased to 20 m, the same anomaly patterns of the polarization parameters are obtained with the fact that all the shapes of all the polarization parameters become broader, larger and pushed apart (Fig. 4b) compared to (Figs. 3a and 4a). These results clearly indicate that VLF signatures are influenced by the dimension of the ore-body such that large ore size will produce broad anomaly signature and vice-versa. Table 2 summarizes the polarization parameters for the inductively coupled model. The differences observed in the amplitudes of polarization parameters may be due to VLF screening by the overburden [46].

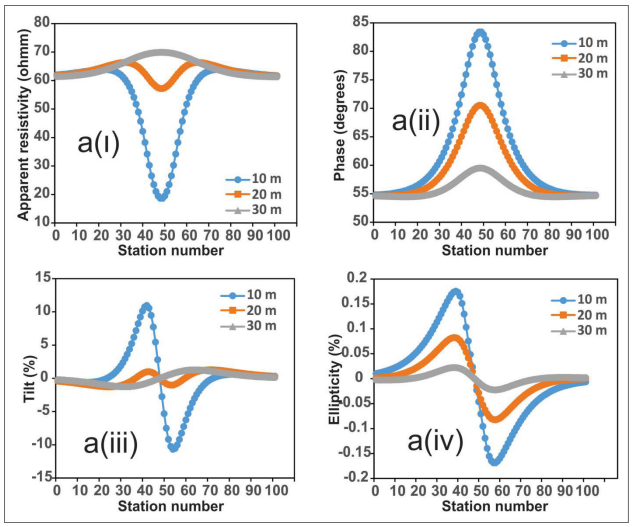

Figure 4a. Computed polarization parameters for a buried conductor model 2 for overburden resistivity of 50 ohm-m, and overburden thicknesses of 10, 20 and 30 m. The upper left panel show resistivity a(i), upper right panel show phase a(ii), lower left panel show the tilt angle a(iii) while the lower right panel show the ellipticity a(iv).

DOI: https://doi.org/10.30564/jgr.v3i1.2809

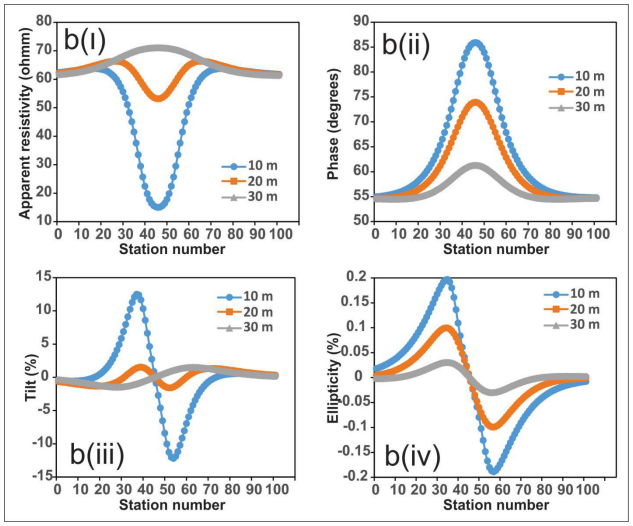

Figure 4b. Computed polarization parameters for a buried conductor model 2 for overburden resistivity of 50 ohm-m, and overburden thicknesses of 10, 20 and 30 m. The upper left panel show resistivity b(i), upper right panel show phase b(ii), lower left panel show the tilt angle b(iii) while the lower right panel show the ellipticity b(iv).

In general, the results indicate that the higher the resistivity of the overburden, the higher and more separated the amplitude of the resistivity (comparing Figs. 3a(i), 3b(i), 3c(i) and 3d(i)) but the lower the amplitude of the phase at various thicknesses of the overburden (comparing Figs. 3a(ii), 3b(ii), 3c(ii) and 3d(ii)). The values of the phase increasingly overlap at increasing resistivity values at increasing depth. The tilt increases with increasing resistivity of the overburden for all depths (comparing Figs. 3a(iii), 3b(iii), 3c(iii) and 3d(iii)) except at 30 m where there is slight decrease. There is a slight decrease in the ellipticity amplitude as the resistivity of overburden is increasing for all depths (comparing Figs. 3a(iv), 3b(iv), 3c(iv) and 3d(iv)). For all polarization parameters, the largest amplitude occurs at overburden thickness of 10 m where the signal is much more enhanced and diagnostic than at deeper depths. This is so because the conductor is closer to the surface. This general decrease in amplitude is possibly due to attenuation of the VLF field by the increasing overburden thickness thus leading to modification and masking of the VLF responses of the underlying conductor. These results show that both the thickness and resistivity of the overburden definitely affect the VLF responses that are obtained in such environment. Tables 1 and 2 summarize the polarization parameters for the conductively coupled model and inductively coupled model respectively.

A noticeable observation is the enhancement of the ellipticity more than tilt angle response which may be due to current channeling [46]. The galvanic contact between the buried ore-body and the overburden allows induced currents flow directly into the buried target. These currents are concentrated mainly in the out-of-phase components from the overburden, whereby the quadrature response exhibits greater enhancement than the in-phase response. Due to sharp attenuation in the surrounding medium and in the overburden, the tilt angle anomaly decays

Table 1. Polarization parameters for Model 1

	Resistivity (Ωm)			Phase (degree)			Tilt (%)			Ellipticity (%)		
Overburden (m)	10 m	20 m	30 m	10 m	20 m	30 m	10 m	20 m	30 m	10 m	20 m	30 m
	Overburden resistivity 50 Ωm											
Minimum	17.6838	49.1637	50.7172	46.9356	46.3086	45.3064	-8.49317	-1.58596	-1.31369	-0.1775	-0.0757	-0.0194
Maximum	48.7902	54.3286	57.9888	77.9628	61.4753	50.2227	8.54294	1.58629	1.31522	0.1839	0.0757	0.0193
Amplitude	31.1064	5.1649	7.2716	31.0272	15.1667	4.9163	17.03611	3.17225	2.62891	0.3615	0.1515	0.0387
	Overburden resistivity 100 Ωm											
Minimum	18.6439	65.41	99.5045	52.5995	52.9348	50.6028	-10.6806	-2.38224	-1.16452	-0.1741	-0.0972	-0.0472
Maximum	64.5836	88.1977	105.946	81.6048	70.7667	59.9395	10.9492	2.34536	1.16487	0.1811	0.0979	0.0472
Amplitude	45.9397	22.7877	6.4415	29.0053	17.8319	9.3367	21.6298	4.7276	2.32939	0.3552	0.1950	0.0944
	Overburden resistivity 200 Ωm											
Minimum	19.0672	74.0256	139.837	56.3922	59.3367	58.2969	-11.7781	-4.0973	-1.0789	-0.1671	-0.1004	-0.0630
Maximum	74.6968	117.179	160.931	83.5608	77.074	69.6217	12.1193	4.0917	1.0689	0.1735	0.1016	0.0632
Amplitude	55.6296	43.1534	21.094	27.1686	17.7373	11.3248	23.8974	8.189	2.1477	0.3406	0.2019	0.1262
	Overburden resistivity 500 Ωm											
Minimum	19.2858	78.5419	163.307	59.0416	64.7409	66.4451	-12.4533	-5.2844	-2.3802	-0.1597	-0.0958	-0.0654
Maximum	81.4968	139.413	211.469	84.7836	81.4337	77.7679	12.8311	5.3098	2.3766	0.1664	0.0972	0.0658
Amplitude	62.211	60.8711	48.162	25.742	16.6928	11.3228	25.2844	10.5942	4.7568	0.3261	0.1929	0.1312

 DOI: https://doi.org/10.30564/jgr.v3i1.2809

Table 2. Polarization parameters for Model 2

	Resistivity (Ωm)			Phase (degree)			Tilt (%)			Ellipticity (%)		
Overburden (m)	10 m	20 m	30 m	10 m	20 m	30 m	10 m	20 m	30 m	10 m	20 m	30 m
	Conductor width is 10 m; Overburden resistivity is 50 Ωm; Conductor is 4 m below the overburden											
Minimum	18.6776	57.1934	61.2898	54.7593	54.6243	54.4717	-10.668	-1.2755	-1.2682	-0.1688	-0.0823	-0.0224
Maximum	63.8797	66.3554	69.8971	83.3909	70.5144	59.5018	10.9484	1.2772	1.2698	0.1756	0.0825	0.0223
Amplitude	45.2021	9.162	8.6073	28.6316	15.8901	5.0301	21.6164	2.5527	2.5381	0.3443	0.1648	0.0448
	Conductor width is 20 m; Overburden resistivity is 50 Ωm; Conductor is 4 m below the overburden											
Minimum	15.0397	53.1639	61.3067	54.7801	54.6371	54.4688	-12.2005	-1.5754	-1.4892	-0.1741	-0.1888	-0.0992
Maximum	63.7606	66.3253	71.0254	85.9187	73.9432	61.2662	12.5054	1.5350	1.4905	0.1811	0.1966	0.0996
Amplitude	48.7209	13.1614	9.7187	31.1386	19.3061	6.7974	24.7059	3.1104	2.9797	0.3552	0.3855	0.1988

more rapidly compared to ellipticity as depth is increased. Moreover, at depth 30 m (representing large depths) for overburden resistivity of 100 Ωm and below (more conductive than 200 and 500 Ωm), the tilt angle changes sign (Figs. 3a(iii), 3b(iii), and 4a(iii)). [45] showed that phase shifts leading to a total reversal of the in-phase response are common with VLF data acquired in a weathered or conductive terrain. The symmetricity of the shapes of the polarization parameters indicates the existence of a vertically dipping structure. The central low resistivity, central high phase values and cross overs of both the tilt and ellipticity curves at station 50 reflect the position and top of the buried ore-body. The buried ore-body that has direct galvanic contact with the overlying overburden would have large anomaly signature due to current channeling than the ore-body having no galvanic contact due to current screening. It is therefore suggested that overburden resistivity information should be obtained using other geophysical methods before ruling out some VLF responses obtained in a mineralized zone such as in the study area as non-promising. This is necessary because of the strong influence of overburden resistivity on the anomaly curves. These results correlate with field results shown by [15, 3, 37].

5.3 Depth dependence nature of polarization parameters

Table 3 shows some specific numerical characteristics of the polarization parameters against depth. This is to throw more light on the relationship between the polarization parameters and the depth of burial (overburden thickness) to further explain the issue of attenuation of VLF fields. It can be seen that as the depth of burial of the conductor increases, the polarization parameters fall off more rapidly in model 2 (non-galvanic) than in model 1 (galvanic). This shows that the induced currents in the overburden are actually channeled to the buried conductor when there is a galvanic contact with the overburden hence the polarization parameters are more enhanced in model 1. It is not so when there is no galvanic contact between the two bodies therefore model 2 seems to have less amplitude. The ellipticity signature exhibits a distinct anomaly signature in this environment because it falls off less rapidly with depth than the tilt angle anomaly for both models. This suggests that ellipticity VLF signature should be used along with the conventional in-phase components when prospecting for conductive mineralization found in such environment as the study area. By doing this, mineral prospects could be better detected, evaluated and quantified. Lastly, it is seen that thick overburden suppresses VLF anomaly and hence affects the detectability of the conductor.

Table 3. Depth dependence of polarization parameters for conductively coupled model

Depth	Model 1		Model 2	
h (m)	Tilt (%)	Ellipticity (%)	**Tilt (%)**	**Ellipticity (%)**
6	19.79	24.47	14.87	20.23
10	12.83	16.64	10.95	17.56
20	5.31	9.72	1.28	8.25
30	2.38	6.58	1.27	2.23

5.4 Current density pseudo-sections

We have shown that overburden thickness and resistivity affect the amplitude of polarization parameter signatures thereby inhibiting the detectability of the buried conductor through masking and/or screening. Figures 5 and 6 show the computed real and imaginary equivalent current density (ECD) showing the conductivity distributions with depth in pseudo-section form for various depths (overburden thickness, z =10, 20 and 30 m). Over the conductor, the real part of the equivalent current distribution has only positive values for the two models while the imaginary part has both negative and positive values and the maxima of the current appear right on top of the conductor. For each mode l, the strength of the current density decreases with increase in depth from 0 to 60 m.

DOI: https://doi.org/10.30564/jgr.v3i1.2809

For model 1, there is higher variation in the range of ECD values at 10 m, 20 m and 30 m compared to model2 due to overburden effect. The overburden effect plays out in both the real and imaginary components of the ECD. For instance at 10 m, the real part ECD varies for model 1 (Figure 5a) and model 2 (Figure 6a) between 0 and 4.7%; but at greater depth due to overburden effect, the range in variation is higher in model1 (Figs. 5b and c) compared to model2 (Figs. 6b and 6c). The concentration of the current density shows that currents are actually induced into the conductor and they only concentrate on top of the conductor. Similar current flow patterns are observed both for the conductive and inductive overburden models where the shape, location and depth of the top of the conductor are well resolved compared to the bottom of the conductor. This means that the closer the conductor is to the surface the more resolving it is for both the galvanic and the non-galvanic contacts. In all cases, the shape of the ECD is symmetrical which indicates the dip of the conductor is 90°. The observed extended dome-shaped pattern of the current density confirms the suggestion of [45] that such body tend to have such shape which would provide the interpreter with information on source discrimination. In addition, there is an observable concaving of the shape of the imaginary component of the ECD of the conductor at all depths of the overburden only in model2. This pattern may help in field situations to separate such inductively coupled conductors from the conductive ones. These results indicate that both the pseudo-sections of the filtered real and imaginary components of the ECD serve as effective complementary views to delineate conductively or inductively coupled buried ore-body [42, 45].

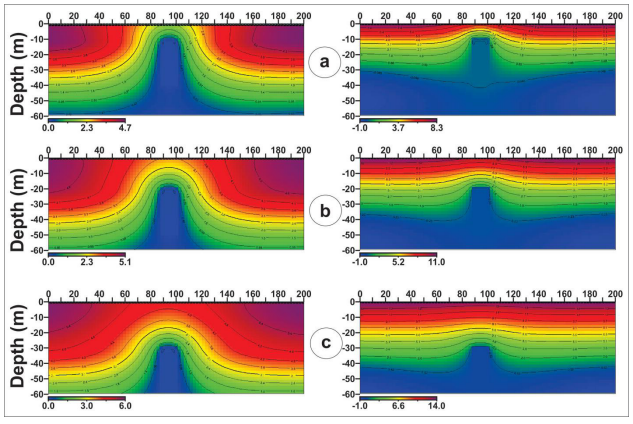

Figure 5. Equivalent current density (ECD) pseudo-section for the conductively coupled overburden model 1 (H-polarization mode). The left panel shows the real component while the left panel shows the imaginary component. The horizontal station spacing is in meters, while ECD is in percentage (%). Overburden thickness is 10 m, 20 m and 30 m in a, b and c respectively.

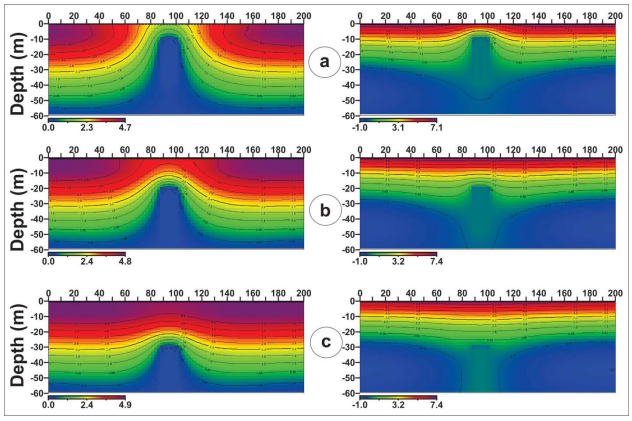

Figure 6. Equivalent current density (ECD) pseudo-section for the inductively coupled overburden synthetic model 2 (H-polarization mode). The left panel shows the real component while the left panel shows the imaginary component. The horizontal station spacing is in meters, while ECD is in percentage (%). Depth to the top of the conductor is 10 m, 20 m and 30 m in a, b and c respectively.

6. Conclusions

On the basis of the numerical VLF modeling studies, the synthetic VLF characteristics of lead-zinc lode found in southeastern Nigeria were computed. The computed model responses are expected to provide mineral explorers with some typical sections to aid in quick identification of the anomaly caused by such deposits found in sedimentary terrain as the study area. The zero crossover point of the tilt angles and ellipticity were shown to indicate the position of the ore-body as the inflection of their signs from positive to negative occurs right on top of the conductor. The minimum of the computed resistivity and maximum of the phase appear directly over the ore body. From this study, we found out that the thickness and resistivity of the overburden medium overlying the mineralized zone coupled with the resistivity of the host rock greatly influence the VLF responses obtained. Combination of these factors was shown to suppress and/or mask the signature of the buried ore target, and hence affect the detectability of the conductor in such terrain. The computed equivalent current distributions for various depths using the Karous-Hjelt linear filtering technique provide good insight about the location, depth extent, dip, size and geometry of the conductor. The numerical modeling studies suggest that VLF-EM can be effectively used to explore lead-zinc mineralization in an environment having similar geology as the study area after due consideration to the aforementioned experimental scenarios.

DOI: https://doi.org/10.30564/jgr.v3i1.2809

References

[1] Eze, C. L., Mamah, L. I., and Israel-Cookey, C., 2004. Very low frequency electromagnetic (VLF-EM) response from a lead sulphide lode in the Abakaliki lead/zinc field, Nigeria. Interational Journal of Applied Earth Observation and Geoinformation, 5, 159-163.

[2] Victor, O. M., Onwuemesi, A. G., and Aniwetalu, E. U. 2015. Exploration of Lead-Zinc (Pb-Zn) mineralization using very low frequency electromanetic (VLF-EM) in Ishiagu, Ebonyi State. Journal of Geol. Geosci. 4: 214. DOI:10.4172/2329-6755.1000214

[3] Phillips, W. J., and Richards, W. E., 1975. A study of effectiveness of the VLF method for the location of narrow-mineralised fault zones: Geoexploration, 13, 215-226.

[4] Warnana, D. D., and Bahri, A. S., 2004. On the use of resistivity and VLF method for profiling underground cave in Ngeposari, Semanu Gunung Kidul. In: Proceedings of the 1st International Seminar of Early Warning System. LPPM-ITS, Surabaya, pp. 33-43.

[5] Monteiro-Santos, F. A., Mateus, A., Figueiras, J., and Gonçalves, M. A. 2006. Mapping groundwater contamination around a landfill facility using the VLF-EM method – a case study. Journal of Applied Geophysics, 60, 115-125.

[6] Kaya, M.A., Özürlan, G., and Şengül, E., 2007. Delineation of soil and groundwater contamination using geophysical methods at a waste disposal site in Çanakkale, Turkey. Environmental Monitoring Assessment, 135, 441-446.

[7] Al-Tarazi, E., Abu Rajab, J., Al-Naqa, A., and El-Waheidi, M., 2008. Detecting leachate plumes and ground water pollution at Ruseifa municipal landfill utilizing the VLF-EM method. Journal of Applied Geophysics, 65, 121-131.

[8] Bahri, A.S., Santoso, D., Kadir, W.G.A., Puradimedja, D. D., Tofan, R. M., and Monteiro-Santos, F. A., 2008. Penerapan metoda Very Low Frequency-vertical Gradient (VLF-EM-vGRAD) untuk memetakan Sungai bawah permukaan di daerah karst. In: Proceedings of the 33rd Pertemuan Ilmiah Tahunan Himpunan Ahli Geofisika Indonesia (PITHAGI), pp. 10 - 20.

[9] Gürer, A., Bayrak, M., and Gürer, Ö. F., 2009. A VLF survey using current gathering phenomena for tracing buried faults of Fethiye–Burdur fault zone, Turkey. Journal of Applied Geophysics, 68, 437-447.

[10] Neumann, T., Berner, Z., Stüben, D., Bahri, A. S., and Jaya, M., 2009. Geowissenschaftliche Bewertung von Karsthöhlen für die asserbewirtschaftung in Gunung Sewu. Wasser Wirtsch. 7-8, 31-36.

[11] Sharma, S. P., Anbarasu, K., Gupta, S., and Sengupta, A., 2010. Integrated very low- frequency EM, electrical resistivity, and geological studies on the Lanta Khola landslide, North Sikkim, India. Landslides, 7, pp. 43-53.

[12] Abbas, A.M., Khalil, M.A., Massoud, U., Monterio-Santos, F., Mesbah, H. A., Lethy, A., Soliman, M., and Ragab, E. S. A., 2012. The implementation of multi-task geophysical survey to locate Cleopatra Tomb at Tap-Osiris Magna, Borg El-Arab, Alexandria, Egypt "Phase II". NRIAG Journal of Astronomy and Geophysics. 1, 1-11.

[13] Adelusi, A. O., Ayuk, M. A., and Kayode, J. S., 2014. VLF-EM and VES: an application to groundwater exploration in a Precambrian basement terrain SW Nigeria. Annals of Geophysics, 57, 1, 2014, S0184; DOI: 10.4401/ag-6291.

[14] Sungkono, A. S., Bahri, D. D. W., Fernando. A.M.S, and Bagus. J.S., 2014: Fast, simultaneous and robust VLF-EM data denoising and reconstruction via multivariate empirical mode decomposition. Computer and Geoscience, 67: 125-138.

[15] Paterson, N. R. and Ronka, V., 1971. Five years of surveying with the very low frequency electromagnetic method. Geoexploration, 9, 7-26.

[16] Saydam. A. S., 1981. Very low frequency electromagnetic interpretation using tilt angle and ellipticity measurements. Geophysics, 46, 1594-1605.

[17] Jeng, Y., Lin, M-J., Chen, C-S., and Wang, Y-H. 2007. Noise reduction and data recovery for a VLF-EM survey using a nonlinear decomposition method. Geophysics, vol. 72, No. 5, September-October, pp. F223-F235.

[18] Bayrak, M., and Şenel, L., 2012. Two-dimensional resistivity imaging in the Kestelek boron area by VLF and DC resistivity methods. Journal of Applied Geophysics, 82, pp. 1-10.

[19] Lowrie, W., and West. G. F., 1965. The effect of conducting overburden on electromagnetic prospecting measurements. Geophysics, 30, 624-632.

[20] Lajoie, J. J., and West. G. F., 1976. The electromagnetic response of a conductive inhomogeneity in a layered earth. Geophysics, 41, 1133-1156.

[21] Joshi, M. S., Gupta, O. P., Negi, J. G., 1984. Scale-model response of a thin vertical conductor below a conductive, inductive, or laterally inhomogeneous over-burden layer. Geophysics, 49, 2159-2165.

[22] Babu, V. R, Ram, S. and Sundararajan, N. 2007. Modeling and inversion of magnetic and VLF-EM data with an application to basement fractures: A case study from Raigarh, India. Geophysics, Vol. 72, No. 5;

DOI: https://doi.org/10.30564/jgr.v3i1.2809

p. B133–b140.10.1190/1.2759921.

[23] Akande, S. O., and Mucke, A., 1989. Mineralogical, textural and paragenetic studies of the Lead-Zinc-Copper mineralization in the lower Benue Trough (Nigeria) and their genetic implications. Journal of African Earth Science, 9, 23-29.

[24] Akande, S. O., and Mucke, A., 1993. Coexisting copper sulphides and sulphosalts in the Abakaliki Pb-Zn deposit, lower Benue Trough (Nigeria) and their genetic significance. Mineralogy and Petrology, Volume 47, Issue 2-4, pp 183-192.

[25] Benkhelil, J. 1987. Cretaceous deformation, magmatism and metamorphism in the lower Benue Trough, Nigeria. Geological Journal, 22, 467-493.

[26] Etim, O.N., Louis, P., and Maurin, J.C., 1988. Interpretation of electrical sounding on the Abakaliki lead–zinc and brine prospects, S.E. Nigeria: Geological and genetic implications. Journal of African Earth Science, 7 (5-6), 743-747.

[27] Orajaka, S., and Nwachukwu, S.O., 1968. Combined electromagnetic and geochemical investigations in Ameri lead-zinc area. Journal of Mining Geology, 3, 49-52.

[28] Olade, M. A and Morton, R. D. 1985. Origin of lead-zinc mineralization in the southern Benue trough, Nigeria. Fluid inclusions and trace element studies. Mineral Deposita, 20, 76-80.

[29] Mamah, L. I., and Eze, L.C., 1988. Electromagnetic and ground magnetic survey over zones of lead-zinc mineralization in Wanakom (Cross River State). Journal of African Earth Science, 7, 749-758.

[30] Coppo, N., Schnegg, P-A., Defago, M., and GSCB. 2006. Mapping a shallow large cave using a high-resolution very low frequency electromagnetic method. Proceedings of the 8th conference on limestone hydrogeology. Neuchatel Switzerland - Web edition, N. Goldscheider, J, Mudry, L. Savoy and F. Zwahlen (Eds), 268 pages.

[31] Sinha, A. K., 1990. Interpretation of ground VLF-EM data in terms of vertical conductor models. Geoexploration, 26, 213-231.

[32] Turberg P., and Müller I., 1992. La méthode inductive VLF-EM pour la prospection hydrogéologique gp" eqpvkpw" fw" oknkgw" Ýuuwtg0" Cppcngu" UekgpvkÝswgu" fg" nÓWpkxgtukvfi" fg Dgucp›qp, Mémoire Hors de Série, nº 11, Cinquième Colloque d´Hydrogéologie en Pays Calcaire et en Milieu Fissuré, Neuchâtel, Suisse, 207-214.

[33] Bosch. F. P., and Muller, I., 2001. Continuous gradient VLF measurements: a new possibility for high resolution mapping of karst structures. First Break, 19, 343-350.

[34] Beamish, D. 1998. "Three-dimensional modelling of VLF data", Journal of Applied Geophysics, vol. 39, pp. 63-76.

[35] Sharma. S. P., Biswas, A., and Baranwal. V. C. 2014. Very Low-Frequency Electromagnetic Method: A Shallow Subsurface Investigation Technique for Geophysical Applications. Recent Trends in Modelling of Environmental Contaminants. DOI: 10.1007/978-81-322-178-1_5. 119-32.

[36] Smith, B. D., and Ward, S. H., 1974. On the computation of polarization ellipse parameters. Geophysics, 39, 867-869.

[37] Adepelumi, A. A., Yi, M. J., Kim, J. H. and Ako, B. D. 2006. Integration of surface geophysical methods for fracture detection in crystalline bedrocks of southwestern Nigeria, Hydrogeology Journal, vol. 14, pp. 1284-1306.

[38] Saydam. A. S. 1981. Very low-frequency electromagnetic interpretation using tilt angle and ellipticity measurements. Geophysics, Vol. 46 (11), 1508-1618

[39] Kayode, J. S., A.O. Adelusi, M.N.M. Nawawi, M. Bawallah, T.S. and Olowolafe 2016. "Geo-electrical investigation of near surface conductive structures suitable for groundwater accumulation in a resistive crystalline basement environment: A case study of Isuada, southwestern Nigeria", Journal of African Earth Sciences, vol. 119, pp. 289-302.

[40] Cagniard, L., 1953. Basic theory of the magnetotelluric method of geophysical prospecting. Geophysics, 18 (3), 605-635.

[41] Kaikkonen, P, 1980. Interpretation nomograms for VLF measurements. Acta. Univ. Ouluensis, A. 92, Phys. 17: 1-48.

[42] Karous, M., and Hjelt, S. E., 1983. Linear filtering of VLF dip-angle measurements. Geophysical Prospecting, 31, 782-794.

[43] Chung, S. H., Lee, S. H and Kim, J. H., 1990. Depth presentation of VLF-EM data using digital filtering. Geophysical exploration method development series KR-89-2D-2 of Korea institute of energy and resources, 97-115.

[44]EM2Dmodel, 2002. EM2Dmodel™ version 1.0, Processing and interpretation software for electrical resistivity data. KIGAM, Daejeon, South Korea.

[45] Ogilvy, R. D., and Lee, A. C., 1991. Interpretation of VLF-EM in-phase data using current density pseudo-sections. Geophysical Prospecting, 39, 567-580.

[46] Poddar, M., 1982. Very low-frequency electromagnetic response of a perfectly conducting half-plane in a layered half-space. Geophysics, 47, 1059-1067.

 DOI: https://doi.org/10.30564/jgr.v3i1.2809